BEST AVAILABLE IMAGES

Defective images within this document are accurate representations of the original documents submitted by the applicant.

Defects in the images may include (but are not limited to):

- BLACK BORDERS
- TEXT CUT OFF AT TOP, BOTTOM OR SIDES
- FADED TEXT
- ILLEGIBLE TEXT
- SKEWED/SLANTED IMAGES
- COLORED PHOTOS
- BLACK OR VERY BLACK AND WHITE DARK PHOTOS
- GRAY SCALE DOCUMENTS

IMAGES ARE BEST AVAILABLE COPY.

As rescanning documents *will not* correct images, please do not report the images to the Image Problem Mailbox.

Kinetics of CO_2 Hydrogenation on a K-Promoted Fe Catalyst

Thomas Riedel and Georg Schaub*

Engler-Bunte-Institut, Universität Karlsruhe (TH), Kaiserstrasse 12, 76128 Karlsruhe, Germany

Ki-Won Jun and Kyu-Wan Lee

Chemical Technology Division, Korea Research Institute of Chemical Technology, P.O. Box 107, Yusong, Taejon 305-600, Korea

CO_2 hydrogenation on a K-promoted Fe catalyst was studied in a fixed-bed microreactor between 300 and 400 °C, at 1 MPa, and with modified residence times in the range of 0.042−21.4 g·s/cm^3. For temperatures below 360 °C, organic products almost identical with those found in the traditional Fischer−Tropsch reaction with H_2/CO were found (paraffins and α-olefins). At 400 °C, formation of carbon deposited on the catalyst became a major reaction. Concerning the mechanism of hydrocarbon formation, the effect of residence time resulted in catalyst particle selectivity values for hydrocarbons always higher than zero. This indicates that, besides the two-step reaction mechanism via CO, a direct hydrocarbon formation from CO_2 can occur in principle. With a reaction scheme proposed from these experimental results, a kinetic model was developed using integration and regression features of ASPEN PLUS. Calculated values for CO_2 conversion and CO and total hydrocarbon selectivities agree with the experimental data within a range of error less than 15%.

1. Introduction

Increasing global energy demands during the past decades has caused increases in man-made CO_2 emissions. Although correlation with global temperature effects is not clear, efforts are taken to reduce CO_2 emissions, as was claimed, e.g., at the Third Conference of the Parties (COP-3) in Kyoto in 1997.[1] Besides improving the efficiencies of energy conversion (e.g., in power plants) or energy utilization processes, strategies include secondary measures, e.g., capture, storage, and fixation of CO_2 produced.[2] In this context, chemical utilization of CO_2 in the conversion of H_2 from CO_2 neutral sources to liquid fuels via Fischer−Tropsch (FT) synthesis is a potential way.[3]

Catalytic hydrocarbon synthesis from synthesis gas CO/H_2 recently gained special attention under the catchword "Gas-to-Liquids" as a way for producing liquid fuels from natural gas.[4] Although there has been some progress in understanding the chemistry of CO_2 hydrogenation and in identifying potential catalysts, information about the kinetics of this reaction is not available. This information could be used for feasibility studies regarding the CO_2 utilization potential of this method.

Hydrogenation of CO_2 so far has been studied mainly on catalysts used traditionally for the FT reactions. On silica-supported Ni and Ru catalysts, the main product is methane; only minor amounts of higher hydrocarbons were observed under the reaction conditions applied.[5] For cobalt as an active metal, Riedel et al.[6] studied the effect of varying CO/CO_2 ratios in the synthesis gas. With increasing CO_2 content, the product composition shifted from a typical FT-type (mainly hydrocarbons) to almost exclusively methane. Generally, Co catalysts exhibit no significant activity for the CO shift reaction at moderate reaction temperatures[7] or for the formation of CO via the CO_2 shift reaction. Therefore, the FT regime of specific inhibition of product desorption through strong reversible CO adsorption as a prerequisite on cobalt for the formation of long-chain hydrocarbons cannot be obtained under such conditions.[8]

So far, iron exhibits the most promising properties for hydrogenation of CO_2 to form long-chain hydrocarbons.[9] It is well-known as an active metal in commercial FT synthesis (e.g., in the ARGE catalyst[10]) and is also widely used in commercial CO shift reactors,[11] an aspect which will be addressed below. As a consequence, much attention has been paid in the past on improving the catalytic properties of Fe-based catalysts through the use of different support materials[12] or the addition of promoters, e.g., Mn, Zn.[13,14] The most promising Fe catalysts for CO_2 hydrogenation were obtained using Al_2O_3 as the structural support and potassium as the chemical promoter, applied in concentrations of up to 0.5 mol·K/mol of Fe.[15,16]

Previous studies indicate that hydrogenation of CO_2 proceeds via a two-step reaction mechanism.[5,13,17] In the first step, CO_2 is converted to CO in the CO_2 shift reaction (reverse water gas shift reaction, eq 1). The CO

$$CO_2 + H_2 \rightarrow CO + H_2O \qquad \Delta_R H^0_{300°C} = 38 \text{ kJ/mol} \tag{1}$$

produced in this way reacts subsequently in the FT reaction to form organic products (eq 2). Using a H_2/

$$CO + 2H_2 \rightarrow (CH_2) + H_2O \qquad \Delta_R H^0_{300°C} = -166 \text{ kJ/mol} \tag{2}$$

CO and a H_2/CO_2 synthesis gas, respectively, Schulz et al.[18] compared the changes in catalyst activity and product selectivity during the initial formation/activa-

* To whom correspondence should be addressed. Telephone: +49-(0)721 608 2572. Fax: +49-(0)21 606172. E-mail: georg.schaub@ciw.uni-karlsruhe.de.

10.1021/ie000084k CCC: $20.00
Published on Web 02/10/2001

Table 1. Published Values for Apparent Activation Energies of the CO_2 Shift Reaction (with No Information Given about Rate Constant and Inhibition Parameters)

catalyst	T/°C	E_A/(kJ/mol)	ref
FeSi	250–400	56, 72	Kaspar et al.[36]
FeSi–H	250–400	81	Kaspar et al.[36]
FeSi–K	250–400	68, 98	Kaspar et al.[36]
Fe_3O_4	327–427	~80	Spencer[20]
Fe_3O_4/Cr_2O_3	327–427	~80	Spencer[20]

tion of a K-promoted iron catalyst. The transient behavior observed was nearly identical, comprising a sequence of kinetic regimes (episodes); however, the duration of the different episodes lasted much longer with CO_2. At steady-state conditions, almost the same product composition was obtained with both synthesis gases, indicating that formation of organic products from CO_2 proceeds with CO as the intermediate.

Recently, Fiato et al.[19] proposed by using laser-generated iron carbide catalysts that there is also some contribution possible from the direct hydrogenation of CO_2 (eq 3). This reaction is proposed to proceed via

$$CO_2 + 3H_2 \rightarrow (CH_2) + 2H_2O \qquad \Delta_R H^0_{300°C} = -128 \text{ kJ/mol} \quad (3)$$

dissociative adsorption of CO_2 followed by hydrogenation of the adsorbed carbon species. However, the extent to which this reaction contributes to the overall formation of organic products remains open at the moment.

Concerning the kinetics of the CO_2 shift reaction, only limited information is available. Published experimental data indicate that the reaction is very fast over several metallic and oxidic catalysts, having a rather low activation energy (Table 1) and high reaction rates, in comparison with the CO shift reaction (the reverse reaction).[20] For the CO shift reaction, r_{SH1}, a kinetic rate equation such as that shown in eq 4 is typically used.[21]

$$r_{SH1} = k_{SH1}\frac{p_{CO}p_{H_2O} - p_{CO_2}p_{H_2}/K'_{eq}}{p_{CO} + a_{SH1,H_2O}p_{H_2O}} \quad (4)$$

Here, the effect of chemical equilibrium limitations is considered by introducing the equilibrium constant K'_{eq} (eq 5). Summaries of rate equations for the CO shift

$$\log K'_{eq} = \log\left(\frac{p_{CO_2}p_{H_2}}{p_{H_2O}p_{CO}}\right)_{eq} = \left(\frac{2073}{T/K} - 2.029\right) \quad (5)$$

reaction were published, e.g., by Zimmerman and Bukur.[22]

For the CO_2 shift reaction, no information is available about rate equations. Therefore, an expression analogous to the one for the CO shift reaction was used as the starting point in this study. However, a term accounting for a possible inhibition by CO_2 was added in the denominator (Table 2).

In the FT reaction (eq 2), Dry[23] found that, for a reduced Fe catalyst at 225–265 °C at low conversion and low partial pressure of H_2O, the rate of total synthesis gas conversion is proportional to the partial pressure of H_2. At higher conversion, i.e., when the partial pressures of the products are significant, a more general rate equation should be used as a starting point for kinetic modeling,[24] which is based on the one proposed by Anderson[25] (eq 6). To this equation was

Table 2. General Form of Rate Equations for CO_2 Shift Reaction (r_{SH2}), FT Reaction (r_{FT}), and Direct CO_2 Hydrogenation (r_{DH}) Used in the Present Study

reaction	rate equation
CO_2 shift	$r_{SH2} = k_{SH2}\dfrac{p_{CO_2}p_{H_2} - p_{CO}p_{H_2O}/K_{eq}}{p_{CO} + a_{SH2,H_2O}p_{H_2O} + b_{SH2,CO_2}p_{CO_2}}$
Fischer–Tropsch	$r_{FT} = k_{FT}\dfrac{p_{CO}p_{H_2}}{p_{CO} + a_{FT,H_2O}p_{H_2O} + b_{FT,CO_2}p_{CO_2}}$
direct hydrogenation	$r_{DH} = k_{DH}\dfrac{p_{CO_2}p_{H_2}}{p_{CO} + a_{DH,H_2O}p_{H_2O} + b_{DH,CO_2}p_{CO_2}}$

added in the present study a term for possible inhibiting effects of CO_2 (Table 2).

$$r_{FT} = k_{FT}\frac{p_{CO}p_{H_2}}{p_{CO} + a_{FT,H_2O}p_{H_2O}} \quad (6)$$

Other rate equations were proposed, for example, by van Steen and Schulz[26] and Huff and Satterfield,[27] and summarized by Zimmerman and Bukur[22] and Espinoza et al.[28] In all of these equations, a term for the inhibiting effect of water vapor is included. Only Ledacowicz[29] and Nettelhoff,[30] both from the same research group, considered exclusively the inhibition by CO_2 instead of H_2O. Zimmerman and Bukur[22] studied FT kinetics of two different Fe-based catalysts under identical reaction conditions. Considering the inhibition of both H_2O and CO_2 gave the best results in the case of a precipitated Fe–Cu–K catalyst, whereas inhibition by CO_2 was negligible in the case of a commercial Fe catalyst (Ruhrchemie LP 33/81). Table 3 gives an overview of the kinetic parameters for the FT reaction which can be found in these publications.

Espinoza et al.[28] pointed out that kinetic studies should be performed on the specific catalyst chosen. In addition, they should also cover the proposed range of operating conditions for design and scale-up studies. This is clearly shown by the variety of rate equations, especially the inhibiting effect of H_2O and CO_2, which indicates a strong link between the composition of the catalysts, the reaction conditions applied, and the final rate equation and kinetic parameters obtained.[10] For FT catalysts, highly active for the CO shift reaction (e.g., with K as the promoter[11]), leading to low H_2O and high CO_2 partial pressures, inhibition of CO_2 (and H_2O) should be considered, whereas at high H_2O/CO_2 ratios, the inhibiting effect of CO_2 is minor compared to the effect of water. These findings suggest that in the case of CO_2 hydrogenation an inhibiting effect of H_2O as well as of CO_2 has to be considered in the rate equations for the FT and CO_2 shift reactions. Because no information is available about the kinetics of the direct formation of organic products from CO_2, a rate equation similar to that of the FT-type appears to be appropriate (Table 2).

2. Experimental Section and Data Analysis

2.1. Experimental Procedures. The Fe catalyst used in the present study was prepared through quick precipitation from hot aqueous nitrate solutions of the metals Fe, Al, and Cu, with an aqueous NH_3 solution. The washed, dried (12 h at 120 °C in air), and crushed catalyst was then impregnated with a K_2CO_3 solution.

Table 3. Published Values for the FT Rate Equation As Used in the Present Study (Table 2), Experimentally Determined with H_2/CO Synthesis Gases

catalyst	T/°C	a_{FT,H_2O}	b_{FT,CO_2}	k_{FT}/[mol/(s·g·MPa)]	E_A/(kJ/mol)	ref
Sasol Fe catalyst	225–265	na	0	na	63	Dry[23]
precipitated Fe	270	4.51	0	64.8	(89)[a]	Nettelhoff et al.[30]
fused Fe BASF S6-10	240	0	0.19	36	(81)[a]	Nettelhoff et al.[30]
100/0.3/0.2 Fe/Cu/K	250	4.8	0.33	288	(86)[a]	Zimmerman and Bukur[22]
Fe-based Ruhrchemie LP 3/81	250	4.5	0	136.8	(86)[a]	Zimmermann and Bukur[22]
coprecipitated Fe–Cu–K	300	17.5[b]	0	0.396	66.5[c]	Liu et al.[37]
100/0.015/0.005 Fe/Si/K	270	3.016	0	1432.8[d]	na	Raje and Davis[38]

[a] Apparent activation energy for first-order kinetic rate constant [T = 220–265 °C (Zimmerman and Bukur[22]) and T = 230–250 °C (Nettelhoff et al.[30])]. [b] Heat of adsorption determined to be 65.4 kJ/mol. [c] Preexponential factor $k_{FT,0}$ determined to be 4.38 × 10^5 mol/(s·g·MPa); T = 220–300 °C. [d] k related to the mass of active metal Fe.

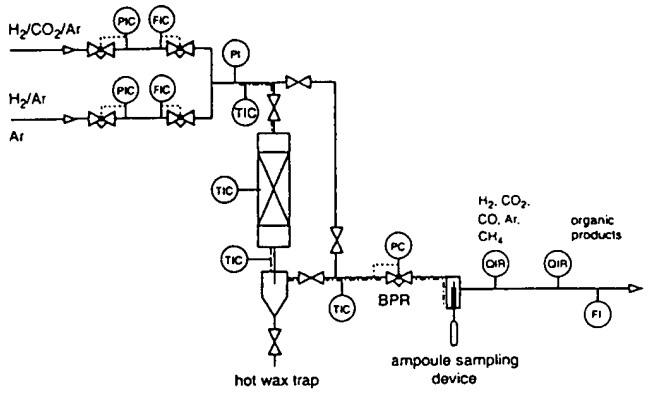

Figure 1. Flow scheme of a fixed-bed microreactor (BPR: back pressure regulator).

Finally, the catalyst was dried again and crushed to a particle size below 100 μm to avoid intraparticle mass-transfer limitations, even in the catalyst pores filled with liquid FT products. The desired composition of the catalyst was 100/13/10/10 $Fe/Al_2O_3/Cu/K$ (mass ratio). Atomic absorption spectroscopy analysis showed a final composition of 100/13.3/10.7/8.9 $Fe/Al_2O_3/Cu/K$. Brunauer–Emmett–Teller surface area was determined as 151 m^2/g for the dried catalyst, which has a bed density of 1.15 g/cm^3.

The relatively high concentration of K was chosen because alkali promotion appears beneficial for the CO_2 hydrogenation reaction.[12] However, too large amounts of K are reported to cause deactivation of the catalyst.[18] Al_2O_3 was used as the structural promoter because it improves iron dispersion, and copper was added to ease the reduction of the catalyst.

CO_2 hydrogenation was studied in a fixed-bed microreactor (flow scheme in Figure 1). The reactor tube (i.d. = 0.9 cm, l = 32 cm) was filled with the desired amounts of catalyst diluted with silica particles (d_P = 250–400 μm) in a weight ratio of catalyst to silica of 1/10. The catalyst particles covered the larger silica particles as an adhering layer; thus, a uniform gas flow at low pressure drop could be achieved, and the high degree of catalyst dilution with the inert material allowed for operation at almost isothermal conditions. The difference in temperature along the reactor middle axis measured with a moveable thermocouple was in the range between ±1 and ±3 °C, depending on the reaction temperature applied and the length of the catalyst bed used (8–15 cm).

After the reactor was filled, the dried catalyst was calcined in Ar (40 cm^3/min, heating with 2 K/min to 400 °C, and holding time 10 h) and subsequently reduced at atmospheric pressure in a H_2/Ar flow (5% H_2 in Ar, 5 cm^3 (0 °C, 0.1 MPa) of H_2 per min and per g of Fe, heating with 2 K/min to 400 °C, and holding time 10 h). The reactor was then cooled to the first reaction temperature of 300 °C, the reaction pressure of 10 bar was adjusted, and the desired reactant gas flow was set. The composition of the gas was $H_2/CO_2/Ar$ = 71.76/24.1/4.14 (mol %); Ar was used as the internal standard for the gas chromatographic (GC) analysis. Initial activation/formation of the catalyst was monitored during a period of several days. Then, after steady-state conditions were ensured for 24 h (also done for every further data point), new reaction conditions were adjusted. When the amount of catalyst (0.1–2.5 g) and the gas flow rate (7–140 cm^3/min) were changed, the modified residence time τ_{mod} was varied between 0.042 and 21.4 g·s/cm^3. After the reproducibility of the experiment was checked, the next temperature, 330, 360, and 400 °C, was set. Analysis of the gases H_2, CO_2, CO, CH_4, and the internal standard Ar was done using an on-line GC with a thermal conductivity detector (TCD). Organic products were analyzed using an ampule sampling technique and adapted GC with a flame ionization detector (FID).[31] The carbon balance was closed within −2 and +5 C % (except at 400 °C as discussed in section 4.1).

2.2. Data Analysis and Definitions. With the data obtained from the GC–TCD analysis, the ratio of the peak areas of the inorganic gases and of methane related to the peak area of the internal standard Ar was calculated. When these ratios were multiplied with earlier determined calibration factors and the exact known molar flow of Ar, the molar flows of these gases were obtained, which were used to calculate the conversion of CO_2 and the yield of CO and CH_4.

The peak areas of the organic products obtained from the GC–FID analysis were referred to the peak area of methane. With the molar flow of CH_4 known from the GC–TCD analysis, the molar flows of the organic products were calculated and used to determine their yields and selectivities on a carbon basis (in C %). A semilogarithmic plot of the mole fraction of organic products against the carbon number gives the Anderson–Schulz–Flory (ASF) plot,[11] where the slope yields the chain growth probability α.

Kinetic rate parameters of CO_2 hydrogenation were obtained by varying the modified residence time expressed as τ_{mod} (eq 7).

$$\tau_{mod} = \frac{m_{cat}}{\dot{V}_{in}(0\ °C, 0.1\ MPa)} \tag{7}$$

Concerning the reactor model to be applied for the kinetic analysis of the experimental data, preliminary theoretical studies suggest that, under the reaction conditions applied, axial dispersion ($Pe_{ax} \sim 2$, $l_r/d_p >$

400, resulting in $Bo_{ax} > 800$) and wall effects ($d_r/d_P > 10$) can be neglected. Because of the small particle size applied, internal mass-transfer limitations are not significant.[18] Although a limited variation in temperature was observed along the reactor axis (max ± 3 °C at a reaction temperature of 400 °C), the assumption of an isothermal ideal plug-flow reactor (PFR) was made. As a result, a steady-state plug-flow model is used for each component i (eq 8). F_i is the axial molar flux in

$$\frac{dF_i}{dx} = \sum_j \nu_{i,j} r_j \rho_{cat} \tag{8}$$

mol/(cm²·s), x, the reactor axial length in cm, $\nu_{i,j}$, the stoichiometric factor of i in reaction j, r_j, the corresponding reaction rate in mol/(g·s), and ρ_{cat}, the catalyst bed density in g/cm³.

Reaction rates are defined on the basis of the total mass of the catalyst used (eq 9). In this equation, ξ_j represents the extent of each reaction.

$$r_j = \frac{1}{m_{cat}} \frac{d\xi_j}{dt} = \frac{1}{m_{cat}} \frac{1}{\nu_{i,j}} \left(\frac{dn_i}{dt}\right)_j \tag{9}$$

3. Numerical Methods

Thermodynamic calculations and kinetic analysis of the experimental data obtained were done using ASPEN PLUS.[32] Equilibrium conversion of CO_2 for a given synthesis gas composition was calculated by minimizing the Gibbs free energy, $\Delta_R G$, for a given set of components allowed to be present at equilibrium. For this purpose, the reactor model RGIBBS in ASPEN PLUS was used.

For kinetic analysis, i.e., determination of kinetic parameter values for CO_2 hydrogenation, the reactor model RPLUG was chosen, which provides a rigorous simulation of an ideal PFR.

Kinetic parameter values were determined via minimization of the sum of square errors f_{min} (eq 10), with N_{exp}, the number of experiments (3, each for one temperature), and N_{data}, the number of data points obtained for varying τ in the each experiment (14, 9, and 7, respectively). As variable Φ, the molar flows of

$$f_{min} = \sum_{j=1}^{N_{exp}} \left(\sum_{k=1}^{N_{data}} \left(\frac{\Phi_k^{exp} - \Phi_k^{calc}}{\sigma_{in}} \right)^2_{reactor,in} + \sum_{l=1}^{N_{data}} \left(\frac{\Phi_l^{exp} - \Phi_l^{calc}}{\sigma_{out}} \right)^2_{reactor,out} \right) \tag{10}$$

H_2 and CO_2 at the reactor inlet and of carbon-containing components CO_2, CO, and C_3H_8 at the reactor outlet were chosen. For the measured data at the reactor inlet and outlet, a standard deviation σ reflecting the experimental errors had to be specified. To fit the calculated data to the experimental data with the regression model DATA FIT from ASPEN PLUS, parameters of the reaction rate equations used and of molar flows at the reactor inlet were varied within a specified range of values, until function f_{min}, calculated with the corresponding flows at the reactor outlet, was minimized.[32] Figure 3 shows the result for a reaction temperature of 300 °C.

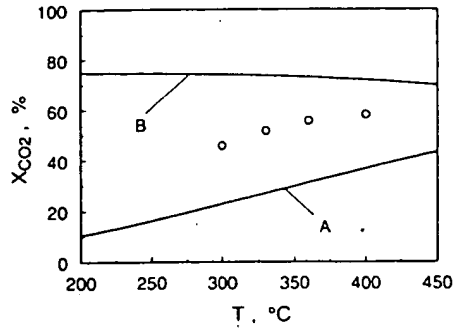

Figure 2. Calculated equilibrium conversion of CO_2 (curves) for an atomic ratio of H/C/O = 6/1/2 [$(p_{H_2}/p_{CO_2})_{in} = 3$] as a function of temperature for p = 1 MPa considering the following components: (A) H_2, CO_2, CO, and H_2O; (B) H_2, CO_2, CO, H_2O, CH_4, and C_3H_8 (representing hydrocarbons); (symbols) experimental data. Catalyst: 100/13/10/10 $Fe/Al_2O_3/Cu/K$. p = 1 MPa, $(p_{H_2}/p_{CO_2})_{in} = 3$, and $\tau_{mod} = 21.4$ g·s/cm³.

4. Experimental Results and Discussion

4.1. CO_2 Conversion, CO, and Total Hydrocarbon Selectivity. According to the main reaction pathway, CO is considered to be first formed via the CO_2 shift reaction and subsequently converted to hydrocarbons. Gibbs free energy calculations indicate that, for the CO_2 shift reaction (eq 1) alone, chemical equilibrium constraints exist in the temperature range of interest here. Equilibrium conversion of CO_2 increases with increasing temperature; however, only about 23% at 300 °C and still less than 45% at 450 °C can be converted to CO (Figure 2). Considering also the formation of hydrocarbons (CH_4 as the most stable one and C_3H_8 representing a relatively stable species of the organic components), a significantly higher equilibrium conversion is possible, however, being still far away from total conversion. Consequently, a limitation of CO_2 shift conversion achievable from thermodynamic considerations is obvious. This clearly shows the disadvantage of CO_2 hydrogenation as compared to CO hydrogenation (traditional FT reaction), where equilibrium values of X_{CO} are practically 100% in the whole temperature range.

Measured CO_2 conversion at the highest value of τ_{mod} applied (ranging from 0.042 to 21.4 g·s/cm³) increased from about 45% at 300 °C to almost 60% at 400 °C (Figure 2). These values are much higher than the calculated equilibrium conversion obtained for the CO_2 shift reaction alone (Figure 2, curve A).

Measured conversion values of CO_2 were found to rise sharply with τ_{mod} for low residence times, followed by a less pronounced increase at longer residence times (Figure 3). Almost doubling of τ_{mod} at high values from 12 to 21.4 g·s/cm³ at 300 °C resulted only in an increase of CO_2 conversion from about 40 to about 45%. This slow increase is possibly due to (a) an approach to the equilibrium conversion of CO_2 (Figure 2, curve B), (b) the decreasing partial pressures of the reactants CO_2 and H_2, and (c) a possible kinetic inhibition by water vapor formed during the reaction. This inhibiting effect of water vapor on an Fe-based catalyst is also known from traditional FT synthesis starting with H_2/CO, where it plays an important role in process design and scale-up strategies, because product inhibition limits the achievable single-pass conversion.[33] Analogous results were obtained for the other reaction temperatures applied, where with increasing temperature the measured CO_2 conversion values approached more and more

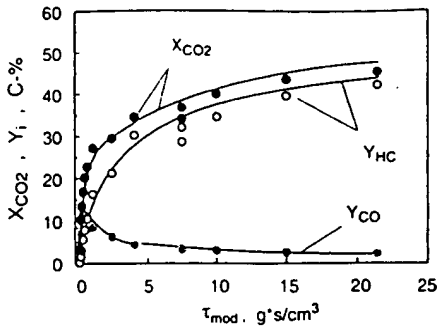

Figure 3. CO_2 conversion and CO and total hydrocarbon (HC) yields versus modified residence time. Catalyst: 100/13/10/10 Fe/Al_2O_3/Cu/K. T = 300 °C, p = 1 MPa, $(p_{H_2}/p_{CO_2})_{in}$ = 3 (data points, experimental; curves, calculated with kinetic model).

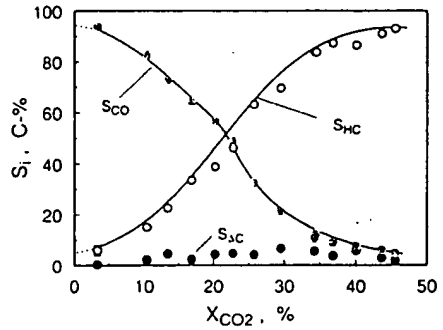

Figure 4. Total hydrocarbon (HC), CO, and "C-loss" ($S_{\Delta C}$) selectivity versus CO_2 conversion. Catalyst: 100/13/10/10 Fe/Al_2O_3/Cu/K. T = 300 °C, p = 1 MPa, $(p_{H_2}/p_{CO_2})_{in}$ = 3, τ_{mod} = 0.042–21.4 g·s/cm³ (data points, experimental; curves, calculated with kinetic model; dashed curves, extrapolation of experimental data to $X_{CO_2} \rightarrow 0$).

the equilibrium conversion. At 400 °C, about 80% of the equilibrium conversion was achieved.

The measured yield values of CO as a function of τ_{mod} exhibit the typical behavior of an intermediate product in a consecutive reaction (Figure 3). At short residence times, a strong increase of Y_{CO} is observed, corresponding to the CO_2 conversion, followed by decreasing values at higher residence times when the consecutive reaction products, i.e., hydrocarbons, are formed as indicated by the curve obtained for the yield of hydrocarbons. The same pattern was found for all reaction temperatures. These results can be seen as evidence for the proposed two-step reaction mechanism for the formation of hydrocarbons from CO_2.[5,13,17]

However, at the lowest CO_2 conversion obtained, respectively the lowest residence time applied, hydrocarbons were also found as products. For S_{HC}, as a measure for particle selectivity, extrapolation toward zero CO_2 conversion (Figure 4) resulted in a value higher than zero, indicating that also hydrocarbons can be formed as a primary product, however, in significantly smaller quantities than CO (5.9 C % versus 93.7 C % at X_{CO_2} = 3.35%). This result is in agreement with Fiato et al.,[19] who proposed a possible direct formation of hydrocarbons from CO_2. $S_{\Delta C}$ in Figure 4, the "C-loss" selectivity (corresponding to adsorbed C, carbid, carbon, chemisorbed organic species, and nonvolatile organic components), represents a sink term in the carbon balance.

The selectivity data obtained for a reaction temperature of 400 °C differ significantly from those obtained at lower temperatures. This can be explained in terms of the "C-loss" selectivity $S_{\Delta C}$. Below 400 °C, values of

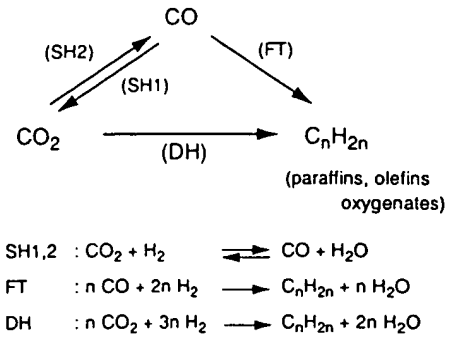

Figure 5. Reaction scheme proposed for CO_2 hydrogenation on a K-promoted Fe catalyst. r_{SH1}: reverse CO_2 shift reaction (CO shift reaction). r_{SH2}: CO_2 shift reaction. r_{FT}: Fischer–Tropsch reaction. r_{DH}: direct formation of hydrocarbons from CO_2 (r_{FT}, r_{DH}: formation of olefins).

$S_{\Delta C}$ were found in the range between −2 and +5 C % (e.g., Figure 4 for 300 °C). However, for 400 °C the value increased drastically to 15–25 C %. The rate of carbon deposition according to the Boudouard reaction (eq 11) was found to be proportional to $p_{CO}/p_{H_2}^2$ and to increase strongly with increasing temperature.[10]

$$CO + CO \rightarrow C + CO_2 \qquad \Delta_R H^0_{300°C} = -173.5\ \text{kJ/mol} \tag{11}$$

At longer residence times, partial pressures of CO at 400 °C were about 2–3 times that for the lower temperatures. Therefore, because no liquid products were formed in the reaction, this "C-loss" selectivity should be almost exclusively attributable to carbon deposited on the catalyst. This is not necessarily in conflict with the fact that the catalyst was still active at the end of the experiments. Dry[34] reported in this context about Fe catalysts used in high-temperature FT synthesis that "a common oversimplification found in the literature is that carbon deposition necessarily resulted in activity loss". After several weeks of operation, there can be twice as much carbon as iron in the catalyst and the activity is still high. In the extreme, there is a "carbon-supported iron catalyst" in the end, with the active iron sites still being readily accessible for the reactants. However, it is clear that secondary reactions at high temperatures can lead to carbon-rich aromatics ("coke"), which results in activity loss.

Because liquid products and olefins are the desired products of CO_2 hydrogenation, the high $S_{\Delta C}$ values, found for 400 °C, clearly show that temperatures above 360 °C should be avoided. It also means that for kinetic modeling an additional reaction for carbon formation must be considered. Therefore, because carbon is an undesired byproduct, only the results obtained for reaction temperatures of 300, 330, and 360 °C will be used to model the formation of hydrocarbons from CO_2 and H_2. As a final conclusion from the experimental results so far, the reaction scheme shown in Figure 5 is proposed for the reaction conditions applied in this study and will be used for the kinetic modeling of the reaction.

4.2. Organic Product Distribution. Among the organic products, methane is thermodynamically most favored. However, it is also the most undesirable product in CO_2 hydrogenation. Therefore, the main objective must be to obtain the lowest possible methane selectivity. Total S_{CH_4} values at 300 °C increased with increasing residence time parallel to the increasing yield of hydrocarbons from 2.5 C % up to a value of about 10

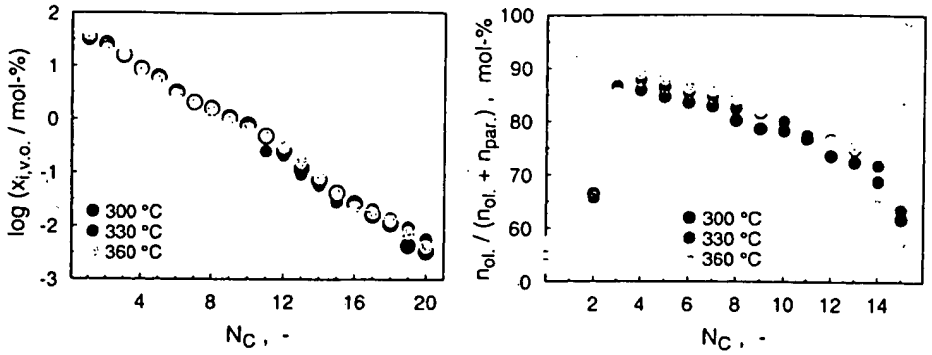

Figure 6. ASF plot of volatile organic products (left) and molar olefin content in linear hydrocarbons (right) versus carbon number from CO_2 hydrogenation with effects of reaction temperature (X_{CO_2} = 46–52%, τ_{mod} = 15–21.4 g·s/cm^3). Catalyst: 100/13/10/10 Fe/Al_2O_3/Cu/K. p = 1 MPa, $(p_{H_2}/p_{CO_2})_{in}$ = 3.

C %. With increasing temperature up to 360 °C, only a slight increase of S_{CH_4} up to 13.5 C % was observed. However, at 400 °C, a significant increase was found; almost 60 mol % of volatile hydrocarbons were CH_4 compared to about 30–40 mol % for the lower temperatures at similar CO_2 conversion values of 46–53%. This result together with the high tendency for carbon formation ($S_{\Delta C} \sim$ 15–25 C %) indicates that at 400 °C the FT regime of long-chain hydrocarbon formation does not prevail anymore.

The total organic product distribution can be described in a simplified way by means of the ASF plot. At 300 °C, the value of the chain growth probability α_1 (C_4–C_7) of about 0.56 was found to be almost independent of the residence time and the CO_2 conversion. In contrast, a slight decrease was found for α_2 (C_{10}–C_{14}), with a value of 0.65 for the longest residence time applied. Although a small effect of residence time was observed, it must be mentioned that the organic products with N_C > 12 amount to less than 3 mol % of the organic products found for the conditions applied here. With the exception of the methane selectivity, the hydrocarbon selectivities and the ASF distribution were only slightly affected by variations in the temperature in the range from 300 to 360 °C (Figure 6, left).

From the traditional FT synthesis starting with H_2/CO, it is known that linear α-olefins and linear paraffins are the main primary products. An adsorbed surface species can form either a paraffin in the gas phase via associative desorption with adsorbed H or an α-olefin via dissociative desorption, leaving an adsorbed H on the catalyst surface.[8] The primary olefin selectivity is about 80%, but α-olefins can undergo secondary reactions such as hydrogenation, double bond shift, and reincorporation in chain growth reactions.[35] The experimentally determined olefin selectivity at 300 °C shows a significant decrease for C_2 with increasing residence time, reflecting the high reactivity of ethylene for secondary reactions and only a moderate decrease for the longer hydrocarbons. At the longest residence time applied, more than 80% of the products up to C_{12} were olefins. Among these olefins, more than 90% were α-olefins. With increasing reaction temperature the olefin content increased slightly (Figure 6, right), an effect which is known from CO hydrogenation,[35] and still more than 90% of the olefins were primary olefins. Besides liquid-saturated hydrocarbon products, also α-olefins are valuable products, which can be used as feedstock for the petrochemical industry. In this respect, the catalytic system investigated in this study exhibits excellent properties with its high α-olefin selectivity.

At 300 °C, the selectivity of oxygenates for C_{3+} was found to be in the range of 5–10%. Almost no effects were observed for varying residence time or reaction temperature. However, within the C_2 fraction, ethanol and acetic aldehyde represented about 50% of the products formed at 300 °C. Their amount was only slightly affected by variations in residence time; however, with increasing reaction temperature, the oxygenates content within the C_2 fraction decreased to about 30% at 360 °C.

5. Kinetic Analysis and Discussion

For the kinetic analysis of the CO_2 hydrogenation data, the model of an ideal PFR operating at isothermal conditions was applied (see section 2). Because of the complex product composition, propane, which has a molecular weight similar to the average of the organic products formed in the reaction ($N_{C,av}$ = 2.5–2.8), was used as the model hydrocarbon for the stoichiometry of the reaction. For the reaction scheme proposed from the experimental results (Figure 5), the following set of differential equations is obtained:

$$CO_2 \qquad \frac{dF_{CO_2}}{dx} = -r_{SH_2}\rho_{cat} - r_{DH}\rho_{cat} \tag{12}$$

$$CO \qquad \frac{dF_{CO}}{dx} = r_{SH_2}\rho_{cat} - r_{FT}\rho_{cat} \tag{13}$$

$$C_3H_8 \qquad \frac{dF_{C_3H_8}}{dx} = \frac{1}{3}(r_{FT}\rho_{cat} + r_{DH}\rho_{cat}) \tag{14}$$

As the starting point for the kinetic analysis with the reactor model RPLUG from ASPEN PLUS, the most general rate equations for CO_2 shift reaction, FT reaction, and direct formation of hydrocarbons from CO_2 (Table 2) were used. A first study with variable exponents for the partial pressures resulted in exponent values close to 1; therefore, the final modeling approach was done using a first-order law for all partial pressures. As a first approximation and in order to minimize the number of parameters to be determined, temperature effects on the adsorption constants were neglected in the temperature range investigated and the values estimated at 300 °C were used for all temperatures.

Table 4 shows a summary of the results for the kinetic parameters which gave the best fit of the experimental data. For all rate equations, the best fit was obtained by considering inhibition terms according to the adsorp-

Table 4. Kinetic Parameter Values As Determined by Regression Analysis for CO_2 Shift Reaction, FT Reaction, and Direct Hydrogenation of CO_2 (Table 2) [Catalyst 100/13/10/10 $Fe/Al_2O_3/Cu/K$; T = 300, 330, and 360 °C, p = 1 MPa, $(p_{H_2}/p_{CO_2})_{in}$ = 3, τ_{mod} = 0.042−21.4 g·s/cm³]

	CO_2 shift	FT	direct hydrogenation
a_{i,H_2O}	65	33	90
b_{i,CO_2}	7.4	2.7	66.0
$k_{i,0}$, mol/(s·g·MPa)	1.51×10^7	2.58×10^8	39.6
E_A, kJ/mol	55	72	20

tion of CO, H_2O, and CO_2. This is in agreement with Zimmerman and Bukur,[22] who, for the traditional FT synthesis with H_2/CO, obtained the best fit of the experimental data with a similar catalyst also by considering the inhibiting effects of H_2O and CO_2 in the FT rate equation. The fact that in this study inhibition by CO_2 has to be considered in all rate equations may be explained, besides by the high partial pressures of CO_2 applied, in terms of the high potassium content of the catalyst. Addition of K increases the surface basicity of the catalyst[15] and therefore favors the adsorption of CO_2, which has an acidic character. The temperature effects on the kinetic rate coefficients k_j were assumed to follow the Arrhenius law (eq 15).

$$k_j = k_{j,0} \exp(-E_A/RT) \qquad (15)$$

The apparent activation energy values obtained (55 kJ/mol for the CO_2 shift reaction and of 72 kJ/mol for the FT reaction) are in the range of those reported in the literature (Tables 1 and 3). However, one has to keep in mind that in the literature the rate equations applied for the FT reaction as well as for the CO_2 shift reaction were different from the ones used in this study. Therefore, a direct comparison is actually not possible, which might explain why in the case of the CO_2 shift reaction the value for the apparent activation energy is on the lower end of the data reported. In the case of direct hydrocarbon formation from CO_2, no published information is available about the kinetics. The resulting parameter values for the latter case are connected to the assumed structure of the rate equation (see Table 2), which must be seen as a first approach.

Taking into account only the reaction rate constants at 300 °C, the value for the FT reaction [70.4 mol/(s·g·MPa)] is more than 100 times higher than the one for the direct hydrocarbon formation [0.59 mol/(s·g·MPa)]. The reaction rate value r_{DH} for reactor inlet conditions (300 °C, p_{H_2} = 0.75 MPa, and p_{CO_2} = 0.25 MPa) is equivalent to r_{FT} for a CO partial pressure as low as $0.0004 p_{CO_2}$. These calculated values and the experimental data obtained at the lowest residence time applied indicate that, for the catalyst used and for the reaction conditions applied, direct formation of hydrocarbons from CO_2 plays only a very minor role compared to the direct formation via CO. For a more detailed and mechanistic clarification, especially for the extent to which the direct formation contributes to the overall hydrocarbon formation and for the determination of a more correct rate equation for r_{DH}, further investigations at low residence time are required, which are currently performed in Korea at KRICT.

The proposed reaction scheme together with the rate equations and kinetic parameters fits the experimental data with good accuracy. This is shown as an example in Figure 3 for CO_2 conversion as well as yields of CO and hydrocarbons at a reaction temperature of 300 °C and in Figure 4 for the corresponding selectivity values. A parity plot for CO_2 conversion (Figure 7) for all reaction temperatures applied reflects the good agreement of the experimental data with values calculated with the model. Except for the lowest residence time applied, the deviation of the calculated from the measured values is in the range of less than ±10%. Also the selectivity data for CO and total hydrocarbons agree with calculated values within an error range of ±15%.

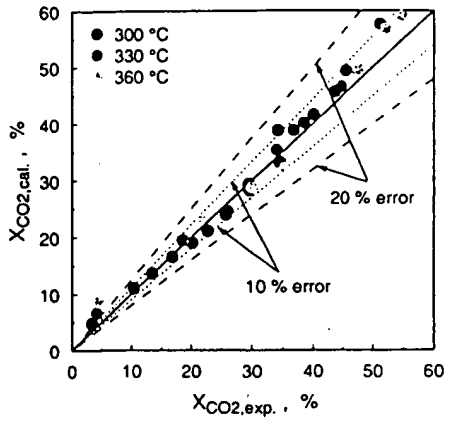

Figure 7. Parity plot for all experimental and calculated CO_2 conversion values at 300, 330, and 360 °C. Catalyst: 100/13/10/10 $Fe/Al_2O_3/Cu/K$. p = 1 MPa, $(p_{H_2}/p_{CO_2})_{in}$ = 3, τ_{mod} = 0.042−21.4 g·s/cm³.

6. Summary and Conclusion

The effect of residence time and reaction temperature on CO_2 hydrogenation was studied in a fixed-bed microreactor at 1 MPa $[(p_{H_2}/p_{CO_2})_{in} = 3]$ using a promoted iron catalyst with the composition 100/13.3/10.7/8.9 $Fe/Al_2O_3/Cu/K$ (mass ratios). The reaction temperature was varied between 300 and 400 °C and the residence time between 0.042 and 21.4 g·s/cm³. Product analysis was achieved by means of GC in connection with a TCD for the inorganic and a FID for the organic components. On the basis of the experimental results, a reaction scheme for CO_2 hydrogenation was proposed. A kinetic model of the overall reaction, including equilibrium constraints, was developed and applied using numerical features of ASPEN PLUS.

The following conclusions can be drawn from the results. Chemical equilibrium calculations display that, for CO_2 hydrogenation, in contrast to the traditional FT reaction with H_2/CO, equilibrium limitations exist for CO_2 conversion. Maximum CO_2 conversion achievable from an equilibrium point of view exhibits a much lower value for the CO_2 shift reaction alone than in a situation where also hydrocarbons are allowed to be present.

The experimental results reflect a two-step reaction mechanism with CO_2 reduction to CO as the primary step (equilibrium-limited with kinetic control) followed by subsequent CO hydrogenation to hydrocarbons (with kinetic control). This sequence of reactions allows for higher overall CO_2 conversion than the CO_2 shift reaction alone.

Separation of both main reactions (CO_2 shift and FT reaction) using two reactors in series would be disadvantageous. For the endothermic CO_2 shift reaction, the first reactor has to be operated at high temperatures to achieve a reasonable CO_2 conversion. Even at about 500 °C, less than 50% of CO_2 can be converted to CO from

an equilibrium point of view. For the second reactor (FT reaction), a much lower temperature is required, and therefore cooling of the reactants would be necessary.

In the temperature range 300−360 °C, paraffins and α-olefins are formed as the main organic products of CO_2 hydrogenation with small amounts of oxygen-containing components. At 400 °C, significant amounts of carbon deposited on the catalyst are formed. Application of the ASF equation to the measured product selectivities leads to chain growth probability values α similar to those found for the traditional FT synthesis with H_2/CO. This means that in CO_2 hydrogenation practically the same organic products can be formed as if the FT reaction starts from CO.

Experiments with varying residence times indicate that extrapolation of measured CO selectivities toward zero CO_2 conversion leads to values of hydrocarbon selectivity higher than zero. This agrees with a hypothesis to be found in the literature[19] that, besides the two-step reaction via CO, also a direct formation of hydrocarbons from CO_2 can take place. However, presently this cannot be seen as evidence that in the intrinsic reaction mechanism a direct formation of hydrocarbons from CO_2 on one active site can occur.

Kinetic modeling of CO_2 hydrogenation was carried out using the reaction scheme proposed as a conclusion from the experimental results. With a PFR model and kinetic parameters determined by nonlinear regression analysis, the experimental data could be fitted with an error of less than 15%. Values found for the apparent activation energies of CO_2 shift (55 kJ/mol) and FT reaction (72 kJ/mol) are in the range of those reported in the literature. Comparing the resulting reaction rates for hydrocarbon formation, it was found that compared to the formation via CO as intermediate direct formation from CO_2 plays only a minor role. The results obtained for this reaction appear to be preliminary; additional work is required. Altogether, with the numerical methods presented, it is possible to model the reaction kinetics of CO_2 hydrogenation on a K-promoted iron catalyst in the PFR used. The resulting kinetics should be regarded as a formal description for the catalytic system investigated in this study.

Acknowledgment

This work was financially supported by the Deutscher Akademischer Austauschdienst (DAAD), and assistance was provided by Myung-Woo Lee from KRICT (Taejon) and Sabina Hug from Engler-Bunte-Institut (Karlsruhe). Both are greatly appreciated.

Nomenclature

a_{i,H_2O} = inhibition coefficient for H_2O in reaction i
av = average
α = chain growth probability
b_{i,CO_2} = inhibition coefficient for CO_2 in reaction i
BPR = back pressure regulator
calc = calculated
d_P = particle diameter, μm
d_r = reactor diameter, cm
$\Delta_R H^0_{300°C}$ = heat of reaction at standard pressure, kJ/mol
$\Delta_R G$ = Gibbs free energy, kJ/mol
exp = experimental
E_a = apparent activation energy, kJ/mol
f_{min} = function to be minimized (eq 10)
F_i = axial molar flux of component i, mol/(cm²·s)
Φ = variable in eq 10
k_j = reaction rate constant for reaction j, mol/(s·g·MPa)
$k_{j,0}$ = preexponential factor in Arrhenius law (eq 15), mol/(s·g·MPa)
K'_{eq} = equilibrium constant of CO shift reaction (eq 5)
K_{eq} = equilibrium constant of CO_2 shift reaction ($=1/K'_{eq}$)
l_r = reactor length, cm
m_{cat} = total mass of dried catalyst, g
$\dot{n}_{HC,i}$ = molar flow of component i, mol/min
$N_{C,i}$ = number of carbon atoms in component i
N_{data} = number of values measured in each experiment (eq 10)
N_{exp} = number of experiments in data set (eq 10)
$\nu_{i,j}$ = stoichiometric coefficient
p_i = partial pressure of component i, MPa
r_{SH1} = reaction rate of CO shift reaction, mol/(s·g)
r_{SH2} = reaction rate of CO_2 shift reaction, mol/(s·g)
r_{DH} = reaction rate of direct hydrocarbon formation, mol/(s·g)
r_{FT} = reaction rate of FT reaction, mol/(s·g)
ρ_{cat} = catalyst bed density, g/cm³
R = gas constant = 8.314, J/(mol·K)
S_i = selectivity of component i, C %
σ = standard deviation for measured values (eq 10)
t = time, s
τ_{mod} = modified residence time (eq 7), g·s/cm³
T = temperature, K, °C
v.o. = volatile organic products
$\dot{V}_i$ = volume flow at 0 °C and 1 bar, cm³/min
x = reactor axial length coordinate, cm
ξ_j = extent of reaction j, mol
X_{CO_2} = conversion of CO_2, %
Y_i = yield of component i, C %

Literature Cited

(1) Malin, C. B. The Kyoto Protocol: A Business Perspective. *Oil Gas J.* **1999**, Jan 19, 33.

(2) Eliasson, B.; Riemer, P.; Wokaun, A. *Greenhouse Gas Control Technologies*; Elsevier Science Ltd.: Kidlington, Oxford, U.K., 1999.

(3) Schaub, G.; Schulz, H.; Riedel, T. Utilisation of CO_2 via catalytic hydrogenation to hydrocarbons—kinetics, selectivity and process considerations. In *Greenhouse Gas Control Technologies*; Eliasson, B., Riemer, P., Wokaun, A., Eds.; Elsevier Science Ltd.: Kidlington, Oxford, U.K., 1999; p 367.

(4) Corke, M. J. GTL technologies focus on lowering costs. *Oil Gas J.* **1998**, Sept 21, 71.

(5) Weatherbee, G. D.; Bartholomew, C. H. Hydrogenation of CO_2 on Group VIII Metals. *J. Catal.* **1984**, *77*, 352.

(6) Riedel, T.; Claeys, M.; Schulz, H.; Schaub, G. Comparative study of Fischer−Tropsch synthesis with H_2/CO and H_2/CO_2 syngas using Fe- and Co-based catalysts. *Appl. Catal. A* **1999**, *186* (1 and 2), 201.

(7) Schulz, H.; Claeys, M.; Harms, S. Effect of water partial pressure on steady-state Fischer−Tropsch activity and selectivity of a promoted cobalt catalyst. *Stud. Surf. Sci. Catal.* **1997**, *107*, 193.

(8) Schulz, H.; van Steen, E.; Claeys, M. Specific Inhibition as the Kinetic Principle of the Fischer−Tropsch Syntheis. *Top. Catal.* **1995**, *2*, 223.

(9) Lee, M.; Lee, J. F.; Chang, C. S. Hydrogenation of Carbon Dioxide on Unpromoted and Potassium-Promoted Iron Catalysts. *Bull. Chem. Soc. Jpn.* **1989**, *62*, 2756.

(10) Dry, M. E. The Fischer−Tropsch Synthesis. In *Catalysis Science and Technology*; Anderson, J. R., Boudart, M., Eds.: Springer-Verlag: Berlin, 1981.

(11) Anderson, R. B. *The Fischer−Tropsch Synthesis*; Academic Press Inc.: Orlando, FL, 1984.

(12) Jun, K. W.; Lee, S. J.; Kim, H.; Choi, M.; Lee, K. W. Support effects of the promoted and unpromoted iron catalysts in CO_2 hydrogenation. *Stud. Surf. Sci. Catal.* **1998**, *114*, 345.

(13) Lee, J. F.; Chern, W. S.; Lee, M. D. Hydrogenation of Carbon Dioxide on Iron Catalyst Doubly Promoted with Manganese and Potassium. *Can. J. Chem. Eng.* **1992**, *70*, 511.

(14) Nam, S. S.; Lee, S. J.; Kim, H.; Jun, K. W.; Choi, M. J.; Lee, K. W. Catalytic Conversion of Carbon Dioxide into Hydrocarbons over Zinc Promoted Iron Catalysts. Proceedings of the 3rd International Conference on Carbon Dioxide Removal, Boston, 1996.

(15) Choi, P. H.; Jun, K. W.; Lee, S. J.; Choi, M. J.; Lee, K. W. Hydrogenation of carbon dioxide over alumina supported Fe–K catalysts. *Catal. Lett.* **1996**, *40*, 115.

(16) Yan, S.; Jun, K. W.; Hong, J. S.; Lee, S. B.; Choi, M. J.; Lee, K. W. Promotion effect of Fe–Cu catalyst for the hydrogenation of CO_2 and application for a slurry reactor. *Appl. Catal. A* **2000**, *194*, 63.

(17) Cubeiro, M. J.; Valderrama, G.; Goldwasser, M. R.; Gonzalez-Jimenez, F.; da Silva, M. C.; Perez-Zurita, M. J. Hydrogenation of CO and CO_2 with K and Mn promoted iron catalysts. *Stud. Surf. Sci. Catal.* **1998**, *107*, 231.

(18) Schulz, H.; Schaub, G.; Claeys, M.; Riedel, T. Transient Initial Kinetic Regimes of Fischer–Tropsch Synthesis. *Appl. Catal. A* **1999**, *186* (1 and 2), 215.

(19) Fiato, R. A.; Iglesia, E.; Rice, G. W.; Soled, S. L. Iron catalyzed CO_2 Hydrogenation to Liquid Hydrocarbons. *Stud. Surf. Sci. Catal.* **1998**, *107*, 339.

(20) Spencer, M. S. On the activation energies of the forward and reverse water-gas shift reaction. *Catal. Lett.* **1995**, *32*, 9.

(21) Moe, J. M. Design of Water-Gas Shift Reactors. *Chem. Eng. Prog.* **1962**, *58*, 33.

(22) Zimmerman, W. H.; Bukur, D. B. Reaction Kinetics Over Iron Catalysts Used for the Fischer–Tropsch Synthesis. *Can. J. Chem. Eng.* **1990**, *68*, 292.

(23) Dry, M. E. Advances in Fischer–Tropsch Chemistry. *Ind. Eng. Chem. Prod. Res. Dev.* **1976**, *15* (4), 282.

(24) Jager, B.; Espinoza, R. Advances in low-temperature Fischer–Tropsch synthesis. *Catal. Today* **1995**, *23*, 17.

(25) Anderson, R. B. Hydrocarbon synthesis, hydrogenation and cyclisation. In *Catalysis*; Emmet, P., Ed.; Reinhold Publ.: New York, 1956; Vol. IV, p 1.

(26) van Steen, E.; Schulz, H. Polymerisation kinetics of the Fischer–Tropsch CO hydrogenation using iron and cobalt based catalysts. *Appl. Catal. A* **1999**, *186* (1 and 2), 309.

(27) Huff, G. A.; Satterfield, C. N. Intrinsic Kinetics of the Fischer–Tropsch Synthesis on a Reduced Fused-Magnetite Catalyst. *Ind. Eng. Chem. Proc. Des. Dev.* **1984**, 23 (4), 696.

(28) Espinoza, R. L.; Steynberg, A. P.; Jager, B.; Vosloo, A. C. Low-temperature Fischer–Tropsch synthesis from a Sasol perspective. *Appl. Catal. A* **1999**, *186* (1 and 2), 13.

(29) Ledakowicz, H.; Nettelhoff, H.; Kokuun, R.; Deckwer, W. D. Kinetics of the Fischer–Tropsch synthesis in the slurry phase on a potassium-promoted iron catalyst. *Ind. Eng. Chem. Proc. Des. Dev.* **1985**, *24* (4), 1043.

(30) Nettelhoff, H.; Kokuun, R.; Ledakowicz, S.; Deckwer, W. D. Studies on the kinetics of Fischer–Tropsch synthesis in slurry phase. *German Chem. Eng.* **1985**, *8*, 177.

(31) Schulz, H.; Nehren, S. Die Herstellung von Gas/Dampf-Eichgemischen für die Gaschromatographie. *Erdöl Kohle Erdgas Petrochem.* **1986**, *39*, 93.

(32) *Aspen Plus Reference Manual, User Guide*; Aspen Technology, Inc.: Cambridge, MA, 1994; Vol. 2, Chapter 19.

(33) Schulz, H. Short history and present trends of Fischer–Tropsch synthesis. *Appl. Catal. A* **1999**, *186* (1 and 2), 3.

(34) Dry, M. E. The Fischer–Tropsch Process—Commercial Aspects. *Catal. Today* **1990**, *6*, 183.

(35) Schulz, H.; Rao, B. R.; Elstner, H. Kohle, Fischer–Tropsch Synthese. *Ullmann's Encyklopädie der technischen Chemie*, 4th ed.; Verlag Chemie: Weinheim, Germany, 1977; Vol. 14.

(36) Kaspar, J.; Graziani, M.; Rahman, A. H.; Trovarelli, A.; Vichi, E. J. S.; da Silva, E. C. Carbon dioxide hydrogenation over iron containing catalysts. *Appl. Catal. A* **1994**, *117*, 125.

(37) Liu, Z. T.; Li, Y. W.; Zhou, J. L.; Zhang, B. J. Intrinsic Kinetics of Fischer–Tropsch Synthesis over an Fe–Cu–K Catalyst. *J. Chem. Soc., Faraday Trans.* **1995**, *91* (18), 3255.

(38) Raje, A. P.; Davis, B. H. Fischer–Tropsch synthesis over iron-based catalysts in a slurry reactor. Reaction rates, selectivities and implications for improving hydrocarbon productivity. *Catal. Today* **1997**, *36*, 335.

Received for review January 24, 2000
Revised manuscript received October 24, 2000
Accepted December 20, 2000

IE000084K